Petroleum Science 19 (2022) 1334–1346

Contents lists available at ScienceDirect

Petroleum Science

journal homepage: www.keaipublishing.com/en/journals/petroleum-science

Original Paper

Contact performance analysis of pressure controller's sealing interface in deep in-situ pressure-preserved coring system

Jia-Nan Li [a], Jun Wang [b, c, *], Yun-Qi Hu [a], Zhen-Xi You [a], Meng Xu [a], Ying-Wei Wang [d], Zu-Jie Zou [e], Qi-Yue Kang [e]

[a] School of Mechanical Engineering, MOE Key Laboratory of Deep Underground Science and Engineering, College of Water Resource and Hydropower, Sichuan University, Chengdu, 610065, China
[b] Guangdong Provincial Key Laboratory of Deep Earth Sciences and Geothermal Energy Exploitation and Utilization, Institute of Deep Earth Sciences and Green Energy, College of Civil and Transportation Engineering, Shenzhen University, Shenzhen, 518061, China
[c] State Key Laboratory of Hydraulics and Mountain River Engineering, College of Water Resource and Hydropower, Sichuan University, Chengdu, 610065, China
[d] State Key Laboratory of Coking Coal Exploitation and Comprehensive Utilization, Pingdingshan Tianan Coal Mining Co., LTD., Pingdingshan, 467000, China
[e] Xi'an Research Institute, China Coal Technology & Engineering Group Corp, Xi'an, 710077, China

ARTICLE INFO

Article history:
Received 19 July 2021
Accepted 26 September 2021
Available online 29 November 2021

Edited by Xiu-Qiu Peng

Keywords:
In-situ pressure-preserved coring
Metal seal
Rough surface
Micro contact

ABSTRACT

The sealing performance of contact interfaces plays the most important role in the design and operation of the in-situ pressure-preserved coring system. To meet the demand of ultra-high pressure-retained coring for oil and gas exploration in deep reservoirs, a quantitative analysis of the contact mechanical behavior of the pressure controller was performed. Based on the micro-contact theory of rough surfaces, a three-dimensional numerical model of the rough contact interface between the valve cover and the valve seat was constructed, and the micro-contact behavior of the metal contact surfaces was comprehensively studied. The results show that the actual contact area of the valve interface increases with the increase of surface roughness before the critical contact point, but decreases after that. Compared with the real contact model with double rough surfaces, although the simplified hard-contact model with a single rough surface can reflect the micro-contact behavior of the rough surface to a certain extent, it cannot truly reveal the microchannel morphology between the sealing interfaces under pressure. Therefore, the realistic double-rough-surface model should be recommended to evaluate the sealing performance of coring tools, particularly for high pressure conditions. The material properties of valves have a significant effect on the contact characteristics of rough surfaces, which suggested that the actual contact area decreases with the increase of the elastic modulus of the contact material under the same loading conditions. The knowledge of this work could help to enhance the seal design of pressure controllers for in-situ pressure-preserved coring.

1. Introduction

During the last decades, the Earth's shallow resources have almost been exhausted due to the large-scale continuous exploitation of natural resources, and it has become a major global demand to develop deep resources inside the earth (Abid et al., 2015; Fulthorpe et al., 2018; Gao et al., 2021a; Gao et al., 2018; Ingrid and Martin, 2018; Pang et al., 2015; Xie et al., 2019). Deep resources exploitation, however, is quite different from the acquisition of shallow resources, which is generally faced with extremely complicated conditions, such as high geo-stress, high temperature, high pore pressure and strong engineering disturbance (Gao et al., 2020a, 2021b; Xie et al., 2020; Yang et al., 2020a,b). Such extreme conditions pose huge challenges to the efficient and safe development of deep resources since the traditional exploitation theory for shallow resources does hold true in most cases (Gao et al., 2020b). In this context, an in-situ condition-preserved coring (ICP-Coring)

* Corresponding author. Guangdong Provincial Key Laboratory of Deep Earth Sciences and Geothermal Energy Exploitation and Utilization, Institute of Deep Earth Sciences and Green Energy, College of Civil and Transportation Engineering, Shenzhen University, Shenzhen, 518061, China.
E-mail address: junwangxy@gmail.com (J. Wang).

https://doi.org/10.1016/j.petsci.2021.11.022

technology for deep reservoirs has been proposed recently, which can provide a theoretical foundation and technical support for deep resources development. (He et al., 2020; Wan et al., 2019; Xie et al., 2020, 2021). As one of the key technologies, in-situ pressure-preserved coring (IPP-Coring) can not only maintain the initial formation pressure state of the core, but also minimize the loss of oil and gas components in the core, which helps to give more precise estimations of in-situ formation parameters such as reservoir fluid saturation and hydrocarbon content. Therefore, the development and breakthrough of IPP-Coring technology is of great significance for deep resources exploitation (Wu et al., 2020). Currently, the existing pressure coring technology is mainly employed in the field of petroleum geology and marine resources exploitation. Two famous coring devices, Fugro Pressure Corer (FPC) and HY-ACE Rotary Corer (HRC), have a maximum pressure-retained capacity of around 25 MPa, while the pressure-retained capacity of the Pressure Core Barrel (PCB) used in Deep Sea Drilling Project (DSDP) can reach 35 MPa. The best performance coring device is Pressure Core Barrel (PCS) with a pressure-retained capacity of 70 MPa, which has been successfully applied in the Ocean Drilling Program (ODP) (Chen et al., 2013; Dickens et al., 2000; He et al., 2020; Milkov et al., 2004; Schultheiss et al., 2009). In contrast, the pressure-retained coring tool developed by China Great Wall Drilling Company, namely GW-CP194-80A (Yang et al., 2020a,b), shows a pressure-retained capacity of approximately 60 MPa in many tests but without field application (Yang et al., 2020a,b). Technically speaking, although many global achievements have been obtained in the development of the pressure-retained coring technologies, it remains challenging to develop high-performance pressure coring tools with high reliability and bearing capacity to meet the coring requirements of deep drilling, especially in complex formations with ultra-high temperature and high pressure (Gao et al., 2021; He et al., 2019; Lan et al., 2019; Li et al., 2021; Yu et al., 2020).

In the IPP-Coring system, the sealing performance of the pressure controller is the key point to realize sufficient pressure-bearing capacity under deep extreme conditions. The configuration optimization of the pressure controller solely from the macro level can hardly meet the harsh working environment in deep reservoirs, and the mechanism investigation on the micro-contact behavior of the rough surface proves to be a potential approach to strengthen the sealing performance. Regarding to the micro-contact mechanism of rough interfaces, Whitehouse and Archard (1971) pointed out that the morphology altitude of most engineering rough surfaces follows the Gauss distribution with an exponential autocorrelation function. Hu and Tonder (1992) proposed a new simulation method of three-dimensional rough surface based on autoregressive (AR) time series model for micro-contact behavior investigation, which can quickly generate Gaussian or non-Gaussian rough surface with different statistical parameters. To reveal the effect of surface roughness on the gas pressure flow, Ren et al. (2010) simulated the random rough contact surfaces with arbitrary shapes and analyzed the flow behavior of two-dimensional leakage channels. Based on the Gauss distribution function and the exponential autocorrelation function, Lyu et al. (2015) reconstructed the rough surface model of metal gasket sealing structure, and unraveled the influences of rough surface characteristic parameters and contact pressure on the leakage rate of sealing structure. However, the contact models used in the previous literatures are usually simplified as the contact between a rigid plane and a rough surface, which cannot fully reflect the realistic contact behavior of two rough interfaces.

To reveal the realistic contact behavior of the valve sealing interface of the pressure controller, this work first analyzed the macro contact mechanical behavior based on the geometry configuration and the working principle of a pressure-retained controller. Combined with the micro-contact theory of rough surfaces, a three-dimensional contact model considering the rough sealing interface between the valve cover and the valve seat of the pressure controller was constructed. Systematic numerical simulations have been performed to investigate the micro-contact behavior of the metal seal surfaces for different roughness cases, based on which the relationship between the actual contact area of the metal seal surface and the pressure loading was uncovered. According to the practical engineering requirements, the influences of different surface roughness and material properties on the contact behavior of the sealing surface were further revealed, which may provide a theoretical guidance to sealing design and optimization of the in-situ pressure-retained controller under deep extreme conditions.

2. Rough contact model construction of valve interface in pressure-retained controller

2.1. Contact analysis of sealing interface of a new-designed pressure controller

To meet the technical requirements of deep IPP-Coring, a novelty pressure controller has been designed in our recent work based on the principle of cone self-tightening seal, which is mainly composed of a valve cover and a valve seat (Fig. 1a). When the internal core barrel is raised to a certain position, the valve cover will be triggered to turn over, resulting in a rotation of the valve cover from the vertical direction to the horizontal direction. Since a sealing ring is installed between the valve cover and the valve seat, there is a certain sealing clearance between the valve cover and the valve seat. During the working process, the clearance of the sealing interface will diminish gradually as the pressure acting on the valve cover is continuously increased, by which the metal contact seal ultimately works.

During the coring operation, when the IPP-Coring tool accomplishes the coring at the hole bottom, the initial seal is realized as the valve cover closes under the action of the pre-tightening component. The pre-tightening component mainly consists of a spring and a spring barrel. The preload generated by the spring forces the valve cover to close via the spring barrel (see Fig. 1b). Once the IPP-Coring tool is lifted from the hole bottom to the ground, the pressure difference between the interior and exterior of the pressure chamber will be gradually increased due to the decrease of external environmental pressure, so the pressure acting on the pressure controller is also increased.

When the metal seal works on the contact interface between the valve cover and the valve seat (see Fig.2a), a self-tightening conical seal is ultimately formed, and such kind of sealing performance is closely associated with the contact behavior of the metal seal surface. Since the configuration of the valve cover is determined by the intersection of a cylinder and a circular cone, the contact surfaces of the controller are distributed on different curves of the same conical mating surface. As shown in Fig. 2b, A and B are the two limit states positions of the contact between the valve cover and the valve seat on different cutting planes. The valve cover is subjected to the hydraulic pressure inside the IPP-Coring tool, the bearing force from the valve seat, the friction force on the sealing interface, and the gravity. For the sake of simplification, the contact analysis in this paper is only based on the requirement that the structural strength of the valve cover meets the interior hydraulic pressure, so the change of contact area caused by the elastic-plastic deformation of the valve cover is ignored.

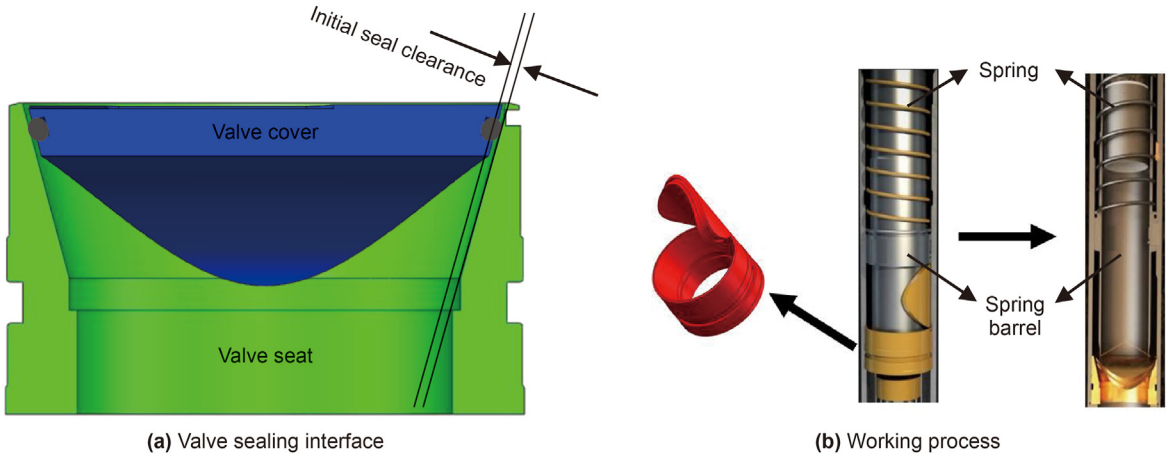

Fig. 1. Sealing principle of the pressure controller.

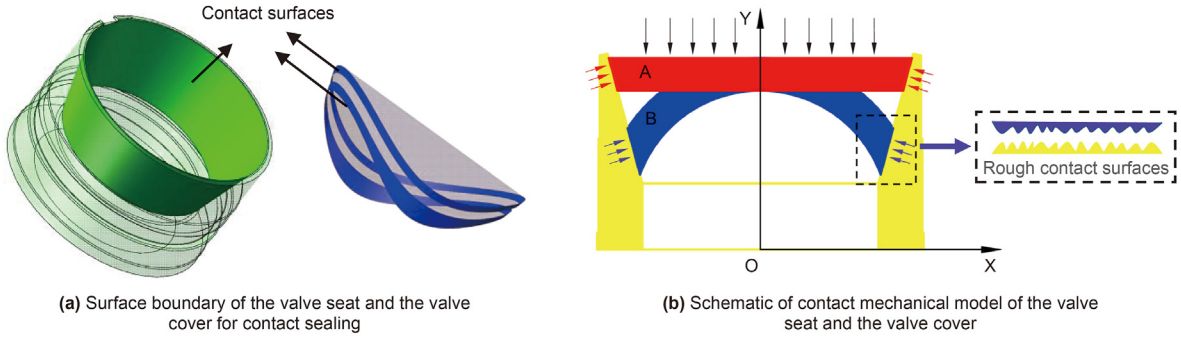

Fig. 2. Physical model of the sealing interfaces of pressure controller.

2.2. Mathematical model of rough sealing interface reconstruction

The valve sealing of the pressure controller is essentially the close contact between the metal surfaces of the seat and the cover. Thus, the micro structure of the contact interface plays a significant role in the sealing performance. Fig. 3 shows the micro topography of the contact seal surface of the valve cover, which demonstrates that the macro smooth contact of the metal sealing surface essentially relies on the micro mechanical contact of rough surfaces.

Generally, a rough-surface contact model is widely applied to investigate the sealing behavior of sealing parts. A three-dimensional rough surface is usually constructed based on statistical principles and mathematical methods, which can be characterized by two key factors. As shown in Table 1, one is the height distribution characteristics, including peaks and valleys, while the other is the spatial distribution feature, which reflects the spatial dependence of each point on the rough surface.

The amplitude parameters mainly reflect the height distribution of rough surfaces. Specifically, the root mean square deviation S_q represents the root mean square value of height distribution in the sampling area, which is defined as

$$S_q = \sqrt{\frac{1}{A}\iint_A z^2(x,y)dxdy} \tag{1}$$

Similarly, the arithmetic mean deviation S_a represents the arithmetic mean value of the absolute value of the height within the sampling area, which is defined as

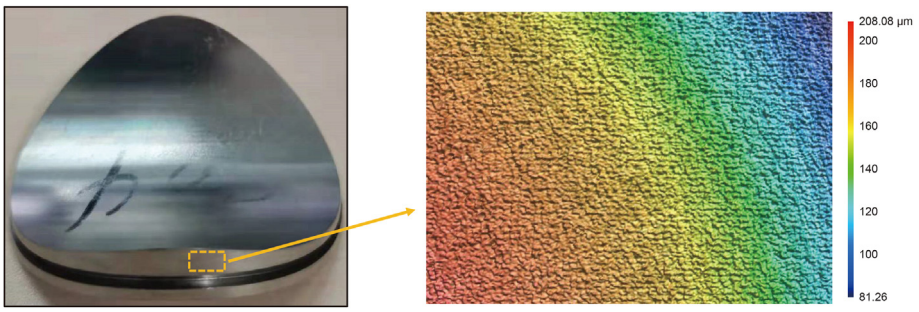

Fig. 3. Micro morphology of the cover contact interface.

Table 1
Roughness characterization parameters.

Parameter type	Parameter name and symbol
Amplitude parameters	Root mean square height S_q; Arithmetic mean height S_a; Maximum height S_z; Skewness S_{sk}; Kurtosis S_{ku}
Spatial parameters	Autocorrelation length S_{al}

$$S_a = \frac{1}{A}\iint_A |z(x,y)|dxdy \tag{2}$$

The skewness S_{sk} indicates the symmetry of the probability distribution of the surface height within the sampling area, and its value reflects the degree of deviation from the center. In Gaussian surface, S_{sk}=0. When $S_{sk} < 0$, the surface height distribution has a left skew associated with a sharp valley. When $S_{sk} > 0$, the surface height distribution has a right skew associated with a sharp peak. Its mathematical expression is

$$S_{sk} = \frac{1}{S_q^3}\left[\frac{1}{A}\iint_A z^3(x,y)dxdy\right] \tag{3}$$

The kurtosis S_{ku} indicates the sharpness of the probability distribution of the surface height within the sampling area. More extreme values of the surface height mean more peaks and valleys on the surface, corresponding to a larger kurtosis, and vice versus. In Gaussian surface, S_{ku} =3. The mathematical expression of the kurtosis is

$$S_{ku} = \frac{1}{S_q^4}\left[\frac{1}{A}\iint_A z^4(x,y)dxdy\right] \tag{4}$$

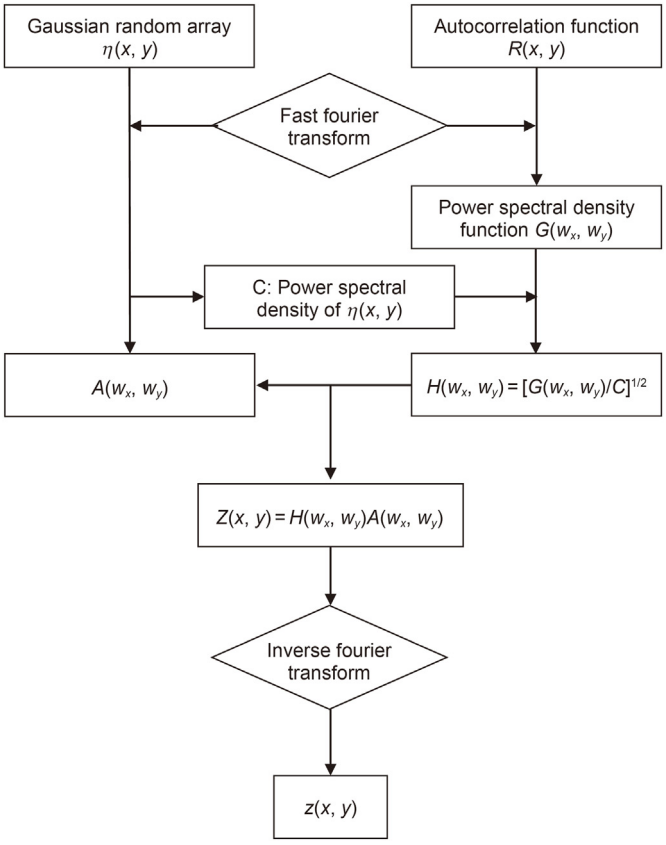

Fig. 4. Numerical reconstruction scheme of rough sealing interfaces.

Since the height distribution of each point on the rough surface is not completely independent, the dependence of each point at different positions can be represented by the autocorrelation function (ACF). The mathematical expression of ACF is as follows

$$R_{zz}(k,l) = E\{z(I,J)z(I+k,J+l)\} \tag{5}$$

where E represents the mathematical expectation, and $z(I, J)$ is the height distribution sequence of rough surface, which is treated as a discrete stationary random process. Besides, k and l are the correlation distances in X and Y directions. In the case of traversal, ACF can be expressed as:

$$R_{zz}(k,l) = \frac{1}{MN}\sum_{I=0}^{N-1}\sum_{J=0}^{M-1} z(I,J)z(I+k,J+l) \tag{6}$$

where M and N represent the number of points on the rough surface in X and Y directions, respectively.

Spatial parameters are further obtained based on the autocorrelation function, which can reflect the horizontal distribution characteristics of rough surfaces. The autocorrelation length S_{al} represents the length in the horizontal direction in which ACF decays to a specific value (generally 0.1).

$$S_{al} = \min_{\tau_x,\tau_y \in R}\left(\sqrt{\tau_x^2+\tau_y^2}\right); R = \left\{(\tau_x,\tau_y) : f_{ACF}(\tau_x,\tau_y) \le s\right\} \tag{7}$$

Where τ_x and τ_y are the horizontal components of the autocorrelation length.

Although the generation of rough surfaces is a random process, the rough surfaces with the same height parameters are usually regarded as equivalent surfaces. According to the previous studies (Colak et al., 2007; Hu and Tonder, 1992; Mu et al., 2018), the surface profile data of milling and grinding parts approximately follows the Gaussian distribution, and the probability density function can be defined as follows:

$$p(z) = \frac{1}{\sqrt{2\pi}\sigma}\exp\left[-\frac{(z-\mu)^2}{2\sigma^2}\right] \tag{8}$$

Generally, the autocorrelation function of a rough surface agrees well with the exponential autocorrelation function (Hu and Tonder, 1992; Masjedi and Khonsari, 2015). Thus, the exponential autocorrelation function is also adopted in this study to construct rough sealing surfaces for contact seal simulations. The exponential autocorrelation function is defined as follows

$$R(k,l) = \sigma^2 \exp\left\{-2.3\left[\left(\frac{k}{\tau_x}\right)^2 + \left(\frac{l}{\tau_y}\right)^2\right]^{1/2}\right\} \tag{9}$$

where σ also known as root mean square roughness, is the standard deviation of the surface height, τ_x and τ_y are the autocorrelation lengths in X and Y directions, k and l are the distances of sampling points in X and Y directions, respectively. Obviously, the spatial distribution of rough surfaces is different with different autocorrelation lengths. The rough surface is isotropic when $\tau_x = \tau_y$, while it is anisotropic if $\tau_x \neq \tau_y$.

Besides, the surface roughness of general engineering

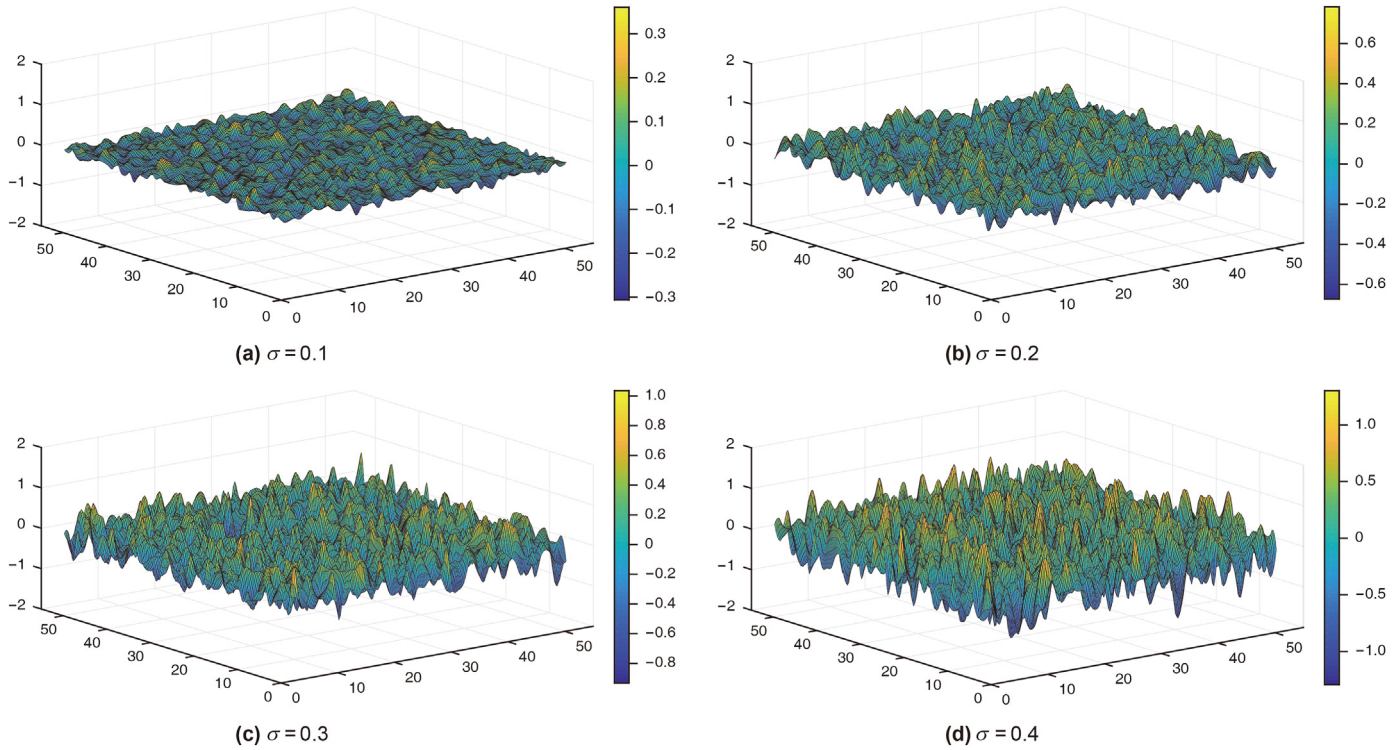

Fig. 5. Reconstructed sealing surfaces with different roughness.

Table 2
Method validation for rough surfaces reconstruction.

Root mean square roughness σ	0.1	0.2	0.3	0.4
Theoretical results of R_a	0.08	0.16	0.24	0.32
Reconstruction results of R_{a0}	0.0795	0.1606	0.2419	0.3183

technology is generally characterized by the arithmetic mean deviation R_a (R_a=S_a), and there is a specific relationship between σ and R_a (Zhao et al., 2006):

$$\sigma = 1.25R_a \tag{10}$$

In this study, inspired by the two-dimensional digital filtering algorithm proposed by Hu (Hu and Tonder, 1992), a micro rough-surface model of the contact interface is constructed by using the specified exponential autocorrelation function and fast Fourier transform (FFT). The numerical construction scheme of rough surfaces is shown in Fig. 4.

From the view of micro contact mechanics, the essence of micro contact of rough surfaces is the physical contact between two asperities. According to the Hertz contact theory, for the sake of simplification, two assumptions are made in the following numerical modeling and analysis: (1) the interaction between two adjacent asperities is negligible; (2) only elastic deformation is considered in the contact process of rough surfaces.

3. Numerical simulation and analysis of contact characteristics of valve sealing interfaces

Due to the fact that the sealing performance is directly affected by the micro contact behavior of the metal sealing interface, the micro surface roughness is one of the decisive impact factors of contact seal performances for a specific metal material. In this paper, stainless steel 304 is selected as the metal material for the rough-surface contact modeling.

3.1. Reconstructed models of contact surfaces with different roughness

To modeling various rough surfaces with different roughness, the root mean square roughness σ was selected as 0.1, 0.2, 0.3 and 0.4, respectively. Four Gaussian rough surface models with different roughness were established by the isotropic surface method, and the model size was set as 50 μm × 50 μm. According to the auto-correlation function and the random array, the height data z (x, y) was obtained by Fourier transform, and the amplitude matrix is generated based on Gaussian distribution, which eventually can be transformed into point cloud (x, y, z). The generated numerical random surfaces with various roughness are shown in Fig. 5.

The above numerical rough surfaces can be discretized by meshing, including 200 × 200 grids and 40401 nodes. The approximate surface arithmetic mean deviation R_{a0} is further evaluated according to the height value of discrete points, which shows a good agreement with the theoretical value R_a calculated by Eq. (10) (see Table 2). Such an agreement demonstrates the validity of our construction method of rough surfaces.

Based on the raw data of rough surfaces with different roughness, the height distribution histograms of discrete points are comparatively displayed in Fig. 6.

As shown in Table 3 and Fig. 6, the arithmetic mean deviation R_{a0} calculated from the constructed models agrees quite well with the theoretical predictions of Eq. (10), and the height distribution histograms of various rough surfaces are approximately consistent with Gaussian distribution. Therefore, the generated rough surfaces based on Gaussian distribution are practical and feasible. The 3D solid model of a rough contact surface can be easily built as shown in Fig. 7.

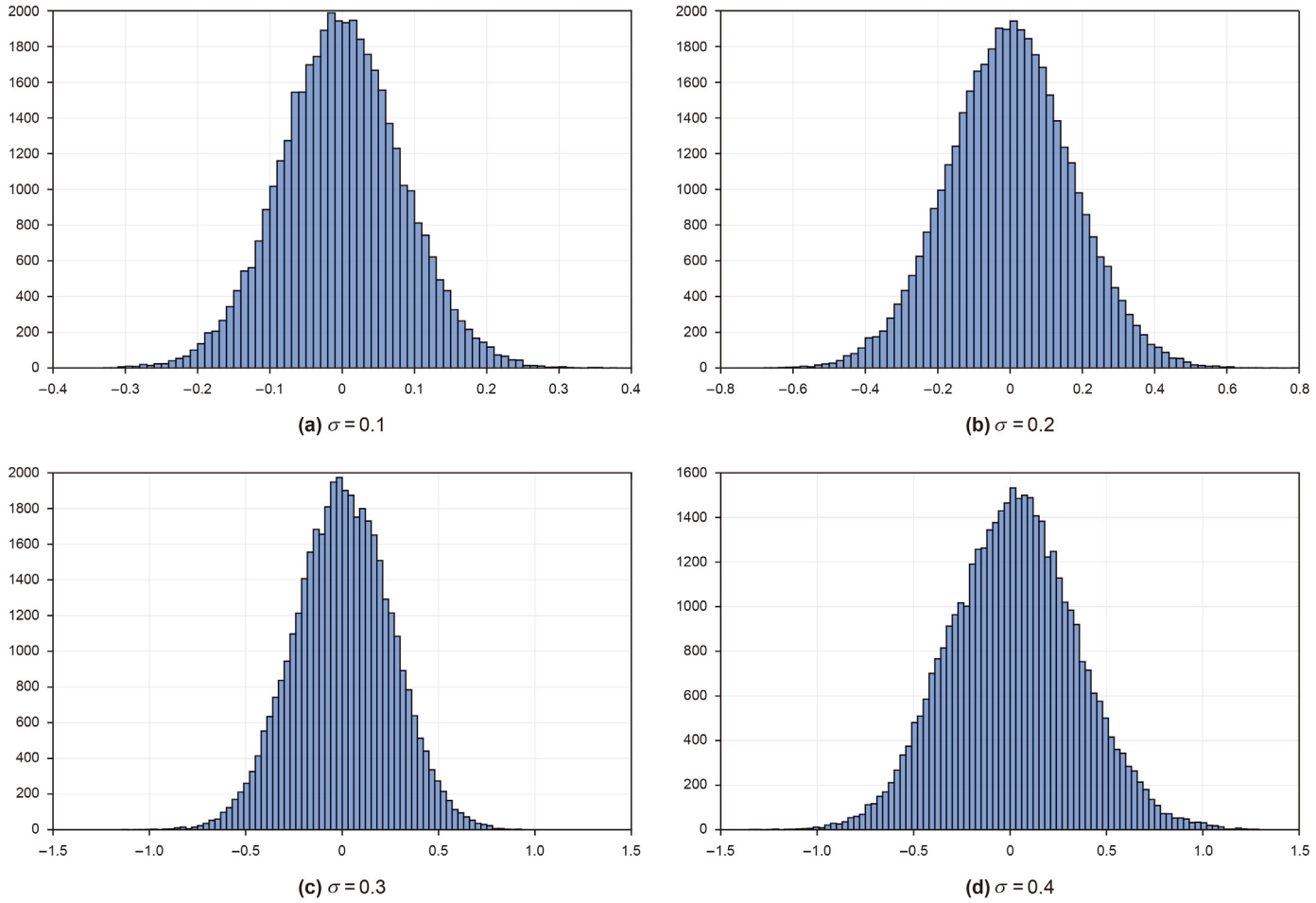

Fig. 6. Height distribution histogram of discrete points on different rough surfaces.

Table 3
Identification of contact surfaces with different roughness.

Contact surfaces	A_0	A_1	A_2	A_3	A_{12}	A_{13}	A_{23}
Root mean square roughness	Rigid plane	0.1	0.2	0.4	0.2236	0.412	0.447

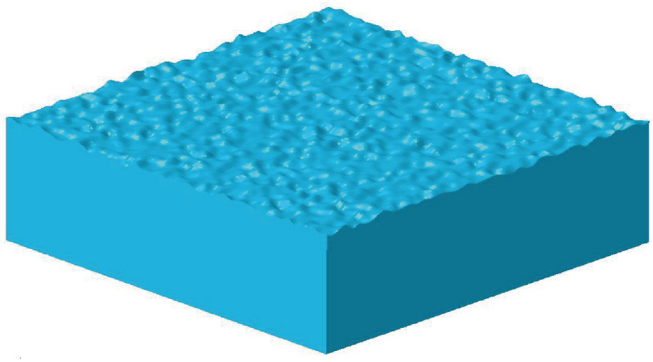

Fig. 7. 3D solid model of a rough surface.

3.2. Effect of surface roughness on micro-contact behavior

To investigate the contact characteristics of micro rough surfaces, the contact between two rough surfaces is usually simplified as the contact between a rough surface and a rigid plane (Ciavarella et al., 2006; Yang and Jackson, 2017; Wang et al., 2021). Based on the Finite Element Method (FEM), the simplified micro-contact model by considering a single rough surface can be established in Fig. 8. The matrix material is stainless steel 304 with the elastic modulus E=200 GPa and the Poisson's ratio v=0.3. The vertical downward load is applied to the rigid plane, the bottom of the domain is fully constrained, and the sides are symmetrically constrained.

As illustrated in Fig. 9, the mean value surface is defined as the virtual surface located on the average height coordinate (z= 0) of the rough surface, and the initial distance between the rigid plane and the mean value surface is set as h_0 = 3.0 μm.

Based on different roughness, the contact models containing a rigid plane and a rough surface are established, and the displacement load is applied to them. The actual contact area and the required contact force F under different contact conditions are calculated. The ratio of actual contact area to ideal contact area is defined as α (area ratio for short), while the displacement variation is H and the loading time is recorded as t.

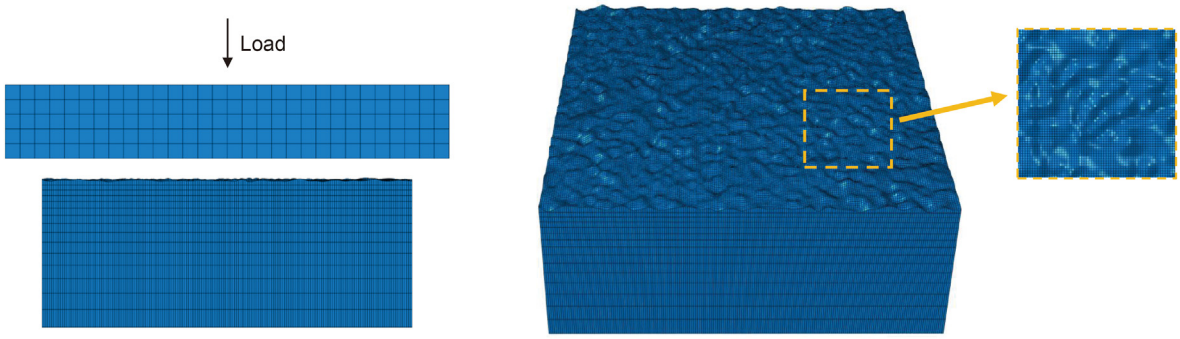

Fig. 8. FEM-based contact model of a single rough surface.

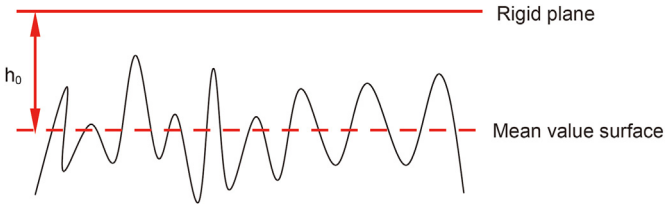

Fig. 9. Schematic of the simplified hard-contact model with a single rough surface.

As can be seen in Fig. 10, due to different roughness, the force required for loading the same displacement is also different. The larger the roughness is, the greater the force required for loading the same displacement is. As the loading process goes on, the contact force required to load the same displacement on the surface with different roughness becomes closer. As can be seen from Fig. 11, because different rough surfaces have different peak heights, the contact time between the rigid plane and the rough surface is also different. With the increase of load, the ratio of actual contact area to ideal contact area increases gradually. The period from 0.5 s to 1.0 s is defined as the contact transition stage. When the loading time t reaches 1.0 s, the contact surfaces with different roughness have the same area ratio, and the loading displacement is equal to the initial value 3.0 μm set between the rigid plane and the mean plane. The contact position can be defined as the contact critical point. With the same load, the actual contact area increases with the increase of surface roughness before the contact critical point, but decreases after it. In practical engineering, the area ratio should be increased as much as possible to enhance the sealing performance.

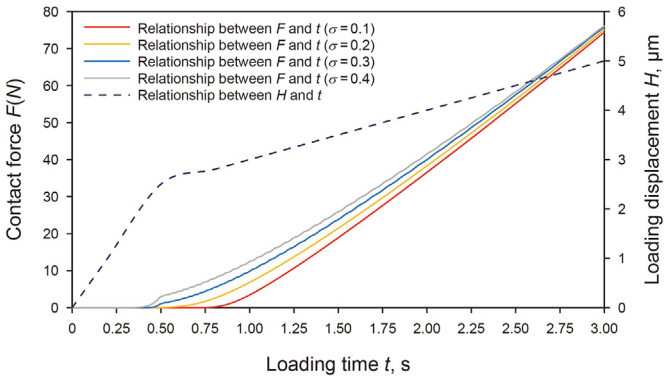

Fig. 10. Variations of the contact force and loading displacement of various reconstructed contact surfaces versus loading time.

Based on different contact area ratios, the variation of rough surface topography with σ=0.1 is shown in Fig. 12. When the contact area is small, there are many pores and micro leakage channels can be formed between the contact surfaces. With the increase of the load, the actual contact area ratio of rough surfaces becomes larger and larger. The microporous channels formed between rough contact surfaces gradually decrease with the increase of the contact area ratio, and the leakage channels gradually decrease or even disappear, so that the leakage rate between contact surfaces gradually decreases.

3.3. Comparative analysis and discussion of the realistic and the simplified contact models

The contact law of rough surfaces can be analyzed by the simplified contact model, but the influence of the simplification on the real contact behavior of double rough surfaces and the construction of microchannels between two rough surfaces has not been studied in detail. Therefore, this paper compares the double rough surfaces contact model and the simplified contact model. According to the actual contact process of double rough surfaces, a real contact model is established to study the contact behavior of sealing interfaces with different roughness under different contact gaps (Fig. 13). Stainless steel 304 is selected as the matrix material with the elastic modulus E=200 GPa and Poisson's ratio ν=0.3. A vertical downward load is applied to the upper body, while a full constraint is prescribed to the bottom of the lower body, and a symmetric constraint boundary condition is applied to both sides of the two contact bodies.

To simplify the contact model of double rough surfaces, it is necessary to establish the contact model between a rigid plane and an equivalent rough surface. In our models, the equivalent root mean square roughness σ_0 of the equivalent rough surface is defined as follows:

$$\sigma_0 = \sqrt{{\sigma_1}^2 + {\sigma_2}^2} \tag{11}$$

Where, σ_1 and σ_2 are the root mean square roughness of the two rough surfaces in the double rough surface contact model respectively. In Table 3, A_0 represents the contact surface of the rigid body, while A_1, A_2 and A_3 represent the real rough surfaces with a roughness coefficient of 0.1, 0.2 and 0.4, respectively. The contact surface A_{12} represents the equivalent rough surface determined by the characterization coefficients of the surfaces A_1 and A_2. Similarly, A_{13} is the equivalent rough surface associated with A_1 and A_3, and A_{23} is the equivalent rough surface associated with A_2 and A_3. According to the contact surfaces with different roughness in Table 3, the corresponding contact models can be established for

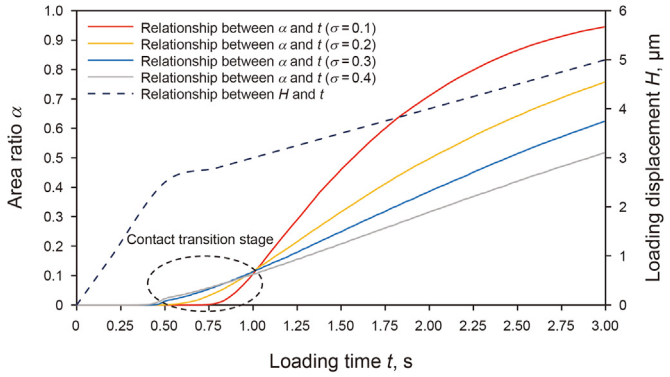

Fig. 11. Variations of the contact area ratio and loading displacement of various reconstructed contact surfaces versus loading time.

comparative analysis as shown in Table 4.

The initial distance between contact surfaces in each group of models is set to 3 μm, and the results are as follows (Fig. 14). Where H is the displacement variation, F_a is the force required for the rough solid to apply the displacement load, and F_b is the force required for the rigid plane to apply the displacement load.

As shown in Fig. 14, when loading the same displacement, the force required by the equivalent simplified contact model is twice that of the realistic contact model with double rough surfaces. This is because the contact force required by the loading displacement is mainly caused by the elastic deformation of the rough solid model itself, while there is only one elastic body in the simplified model, and its deformation is twice that of the double rough surface contact model. The effect of asperity deformation on the force is negligible. Under the double pressure load, the contact area ratio of the simplified contact model is still about 10% smaller than that of the double rough surfaces contact model. However, the variation curve of area ratio and load has an approximate slope, that is, it has

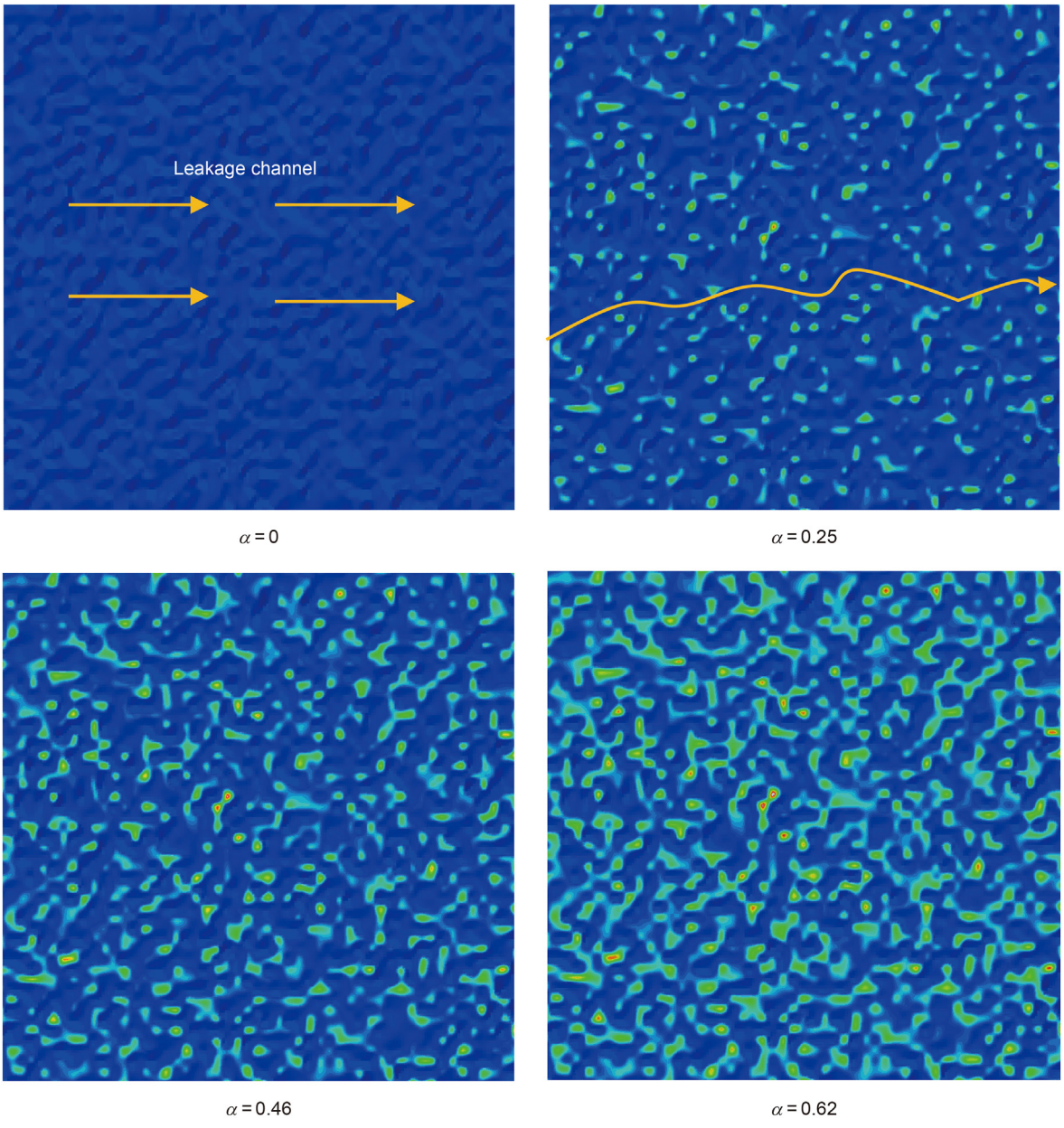

Fig. 12. Variation of rough surface topography during the loading.

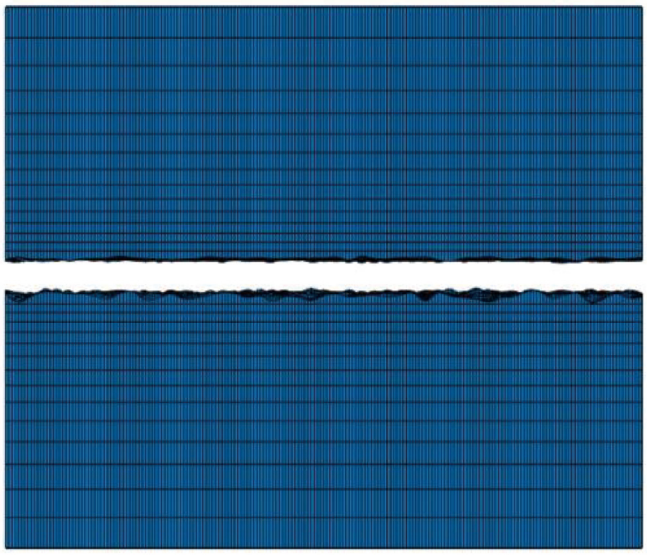

Fig. 13. Realistic contact model with double rough surfaces.

an approximate changeable rule. Therefore, the simplified model can reflect the change law of micro contact behavior of double rough surfaces to a certain extent. If the simplified model is used to evaluate the sealing performance through the actual contact area, the load applied on the contact surface should be corrected, and the specific correction method needs to be further discussed.

To study the sealing performance of the sealing interfaces, in addition to the contact behavior analysis, it is also necessary to analyze the internal microchannel area under the contact effect of double rough surfaces, which helps to give a precise evaluation of the sealing performance. Fig. 15 shows the comparison of the rough surface morphology of the double rough surfaces contact model and the simplified contact model in comparison groups (No. 1 and No. 2) after the sealing interfaces contact. Fig. 15a shows the contact stress contour of the rough surface when the contact area ratio is 0.6, while Fig. 15 (b) shows the contact stress contour of the rough surface when the contact area ratio is 0.4. By comparison, with the same contact area, the contact stress of the rough surface in the simplified model seems larger, which is attributed to the large force applied to it. In the double-rough-surface contact model, the contact stress on the rough surface is smaller with a relatively uniform distribution, because the staggered distribution of random rough peaks makes the initial contact area larger. Meanwhile, the double-rough-surface contact model and the simplified model have completely different surface contact morphology, which implies that the simplified model cannot truly reflect the microchannel structure between the sealing interfaces.

Compared with the real contact model with double rough surfaces, although the simplified hard-contact model with a single rough surface can reflect the micro-contact behavior of the rough surface to a certain extent, it cannot truly reveal the microchannel morphology between the sealing interfaces under pressure. Therefore, the realistic contact model with double rough surfaces should be used to analyze the metal sealing performance.

Table 4
Construction of contact models with different specifications.

Different comparative groups	Comparative group 1	Comparative group 2	Comparative group 3
Double rough surfaces Contact models	A_1+A_2	A_1+A_3	A_2+A_3
Simplified rough surface contact models	A_0+A_{12}	A_0+A_{13}	A_0+A_{23}

4. Contact performance analysis of pressure controller using various manufacturing materials based on practical engineering requirements

As a common structuring material, stainless steel 304 is often used to process the sealing parts of pressure controllers (see Fig. 16). However, in actual engineering, different materials are usually selected to process the valve cover and the valve seat according to the practical sealing requirements of different contact surface combinations. The effect of material properties on micro-contact behavior should be revealed. Based on the realistic contact model with double rough surfaces, various contact models with different material properties have been constructed and analyzed in this section.

According to the characteristics of random distribution, two rough surfaces with σ=0.2 are generated, which have the same statistical parameters but different surface morphology. To comparatively study the contact behaviors of different sealing interfaces with different materials, stainless steel 304 was prescribed to model the valve seat, while three metal materials, including stainless steel 304 (E=200 GPa, v=0.3), aluminum alloy 7075 (E=70 GPa, v=0.3) and titanium alloy TC11 (E=120 GPa, v=0.3), were selected for different valve covers modeling. The corresponding double-rough-surface contact models were constructed for analysis (Fig. 17), and the numerical simulation results are discussed as follows.

As can be seen from Fig. 18, when $t = 0.5$ s, two rough surfaces of the sealing interfaces start to contact. With the increase of displacement load, the actual contact area increases gradually. The rough surfaces combination made of stainless steel 304 has a relatively small actual contact area. But in general, with the same displacement load, the combinations of rough contact surfaces with different material properties have approximately equal actual contact areas. As can be seen in Fig. 19, when the same displacement is applied, the greater the elastic modulus of the material, the greater the force required. In summary, the material properties of valves have a significant effect on the contact characteristics of rough surfaces. When the material properties of one rough surface are determined, with the same force load applied, the larger the elastic modulus of the other rough surface is, the smaller the actual contact area is. On the premise of meeting the compressive strength, the sealing performance can be improved to a certain extent by properly selecting the material with low elastic modulus to process the sealing parts.

5. Conclusions

To reveal the contact behavior of the valve sealing interface of the pressure controller, this work has presented a 3D reconstruction method for contact surfaces with different roughness, based on which a series of numerical simulations were conducted for micro-contact mechanical analysis. The difference in contact characteristics between the simplified and the real contact models was comparatively discussed. The main conclusions are summarized as follows:

(1) Based on the structure analysis and sealing principle of the pressure controller, the numerical model of the micro rough sealing interface can be reconstructed by using a two-dimensional digital filtering algorithm, and the 3D finite element models can be further established to analyze the

contact characteristics of the sealing surfaces with different roughness. With the increase of surface roughness, the actual contact area of the sealing interface increases when the loading is less than the critical contact pressure but decreases after the critical point. For practical engineering applications, it is suggested to enhance the contact area ratio as high as possible for strong sealing performance.

(2) According to the comparative analysis of the simplified contact model and the real contact model considering double rough surfaces, the contact area ratio of the simplified model is about 10% smaller than that of the double rough surfaces contact model under the same loading displacement. A clear discrepancy of contact morphology is also observed between the simplified model and the elaborated model. Although the simplified model can reflect the general characteristics of micro contact behavior of the double rough surfaces to some extent, it is difficult to reveal the real evolution process of the micro-contact channels between the sealing interfaces. Therefore, a real contact model considering double rough contact surfaces should be recommended to analyze the sealing performance of pressure controllers especially under high pressure conditions.

(3) In addition to the interface roughness, the mechanical property of the manufacturing materials, such as the elastic modulus, has a significant effect on the contact performance of the valve sealing interfaces. The actual contact area of the rough surfaces will decrease with the increase of the elastic modulus under the same loading conditions. When the ultimate strength of a pressure controller meets the practical demands, the sealing performance can be improved to a certain extent by selecting a suitable material with relatively low elastic modulus for parts processing.

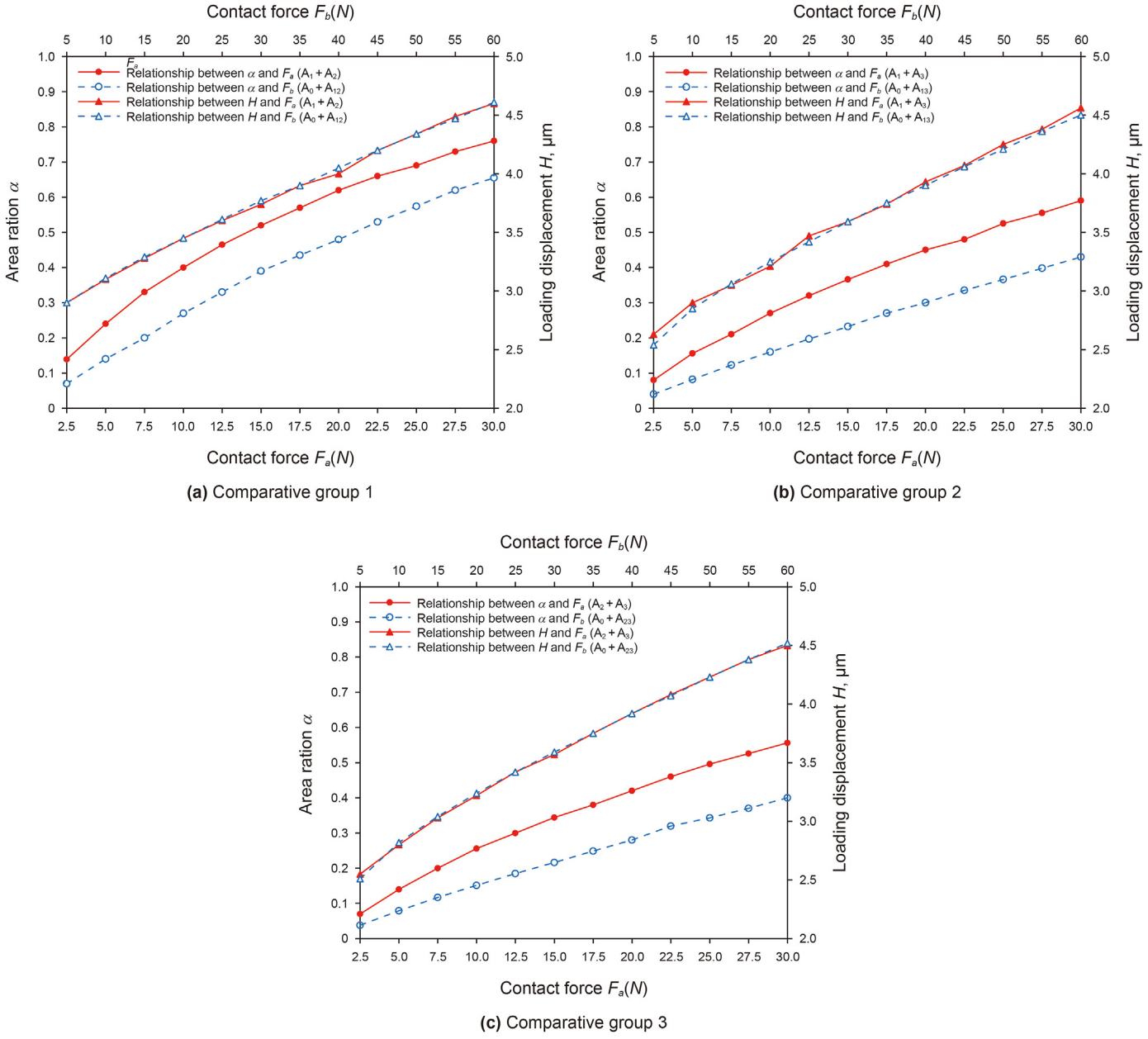

(a) Comparative group 1

(b) Comparative group 2

(c) Comparative group 3

Fig. 14. Comparison results of contact performances of realistic contact models and simplified contact models.

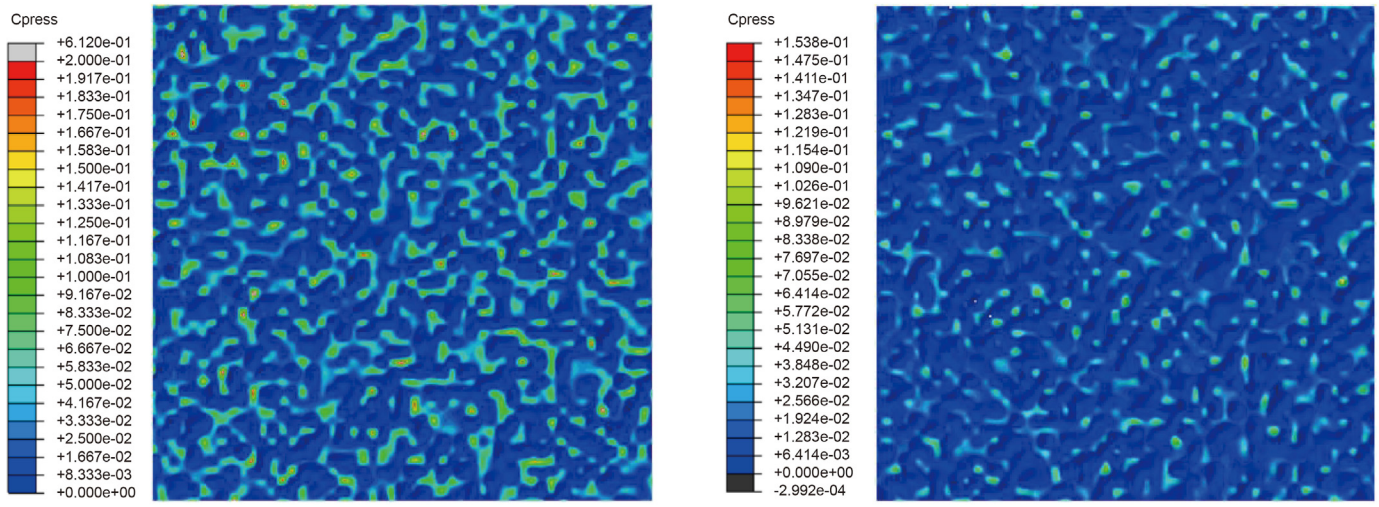

(a) Contact stress and channel morphology of Models A_{12}(left) and A_2(right), ($\alpha = 0.6$)

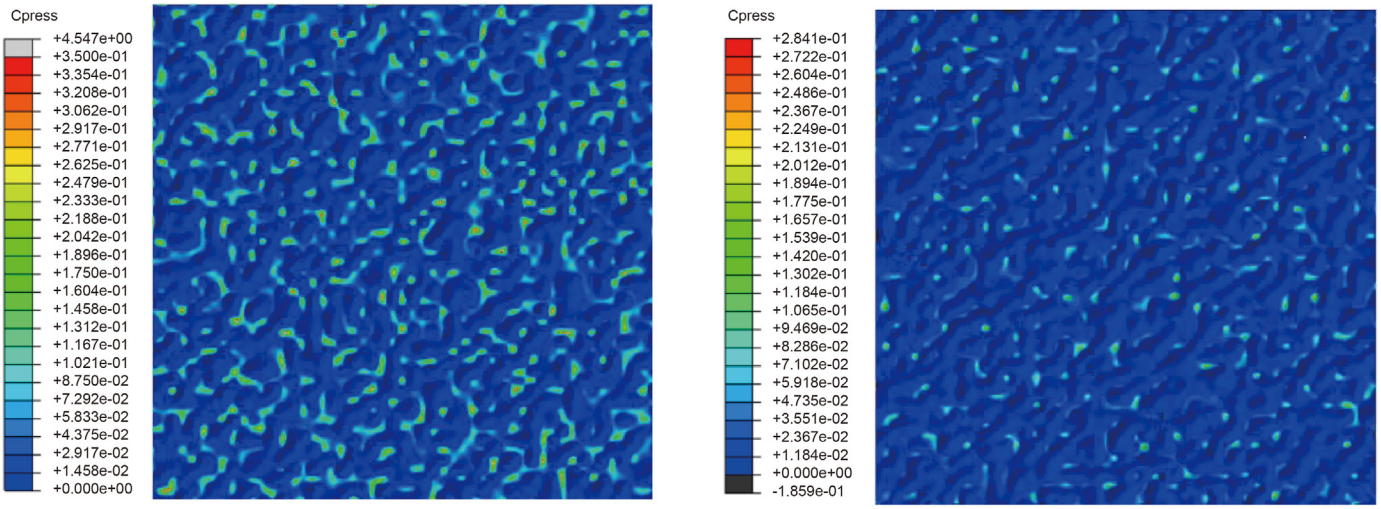

(b) Contact stress and channel morphology of Models A_{13}(left) and A_3(right), ($\alpha = 0.4$)

Fig. 15. Comparison of contact area morphology between the realistic and the simplified contact models.

Fig. 16. Key components of the pressure controller.

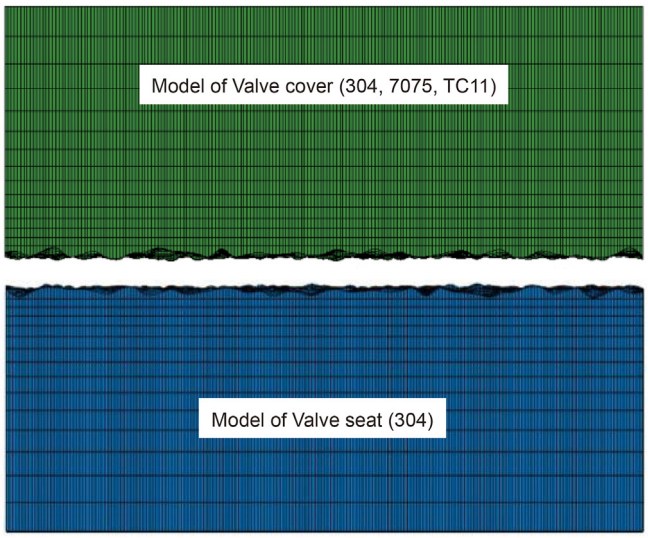

Fig. 17. Contact model with of different manufacturing materials.

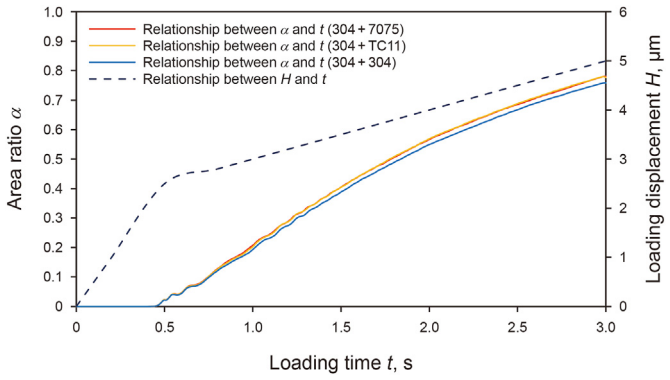

Fig. 18. Variations of the contact area ratio and loading displacement of sealing interfaces versus loading time for different contact materials.

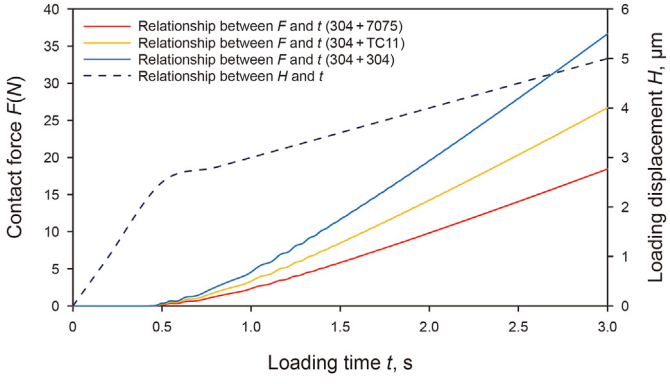

Fig. 19. Variations of the contact force and loading displacement of sealing interfaces versus loading time for different contact materials.

Acknowledgments

The paper was supported by the Program for Guangdong Introducing Innovative and Entrepreneurial Teams (No. 2019ZT08G315), Shenzhen Basic Research Program (General Program, No. JCYJ20190808153416970) and National Natural Science Foundation of China No. 51827901. The financial aids are gratefully acknowledged. All the efforts from the editors and the anonymous reviewers to improve our work are also highly appreciated.

References

Abid, K., Spagnoli, G., Teodoriu, C., et al., 2015. Review of pressure coring systems for offshore gas hydrates research. Underw. Technol. 33 (1), 19–30. https://doi.org/10.3723/ut.33.019.

Chen, J.W., Wei, F., Brian, B., et al., 2013. A long gravity-piston corer developed for seafloor gas hydrate coring utilizing an in situ pressure-retained method. Energies 6 (7), 3353–3372. https://doi.org/10.3390/en6073353.

Colak, O., Kurbanoglu, C., Kayacan, M.C., 2007. Milling surface roughness prediction using evolutionary programming methods. Mater. Des. 28 (2), 657–666. https://doi.org/10.1016/j.matdes.2005.07.004.

Ciavarella, M., Delfine, V., Demelio, G., 2006. A "re-vitalized" Greenwood and Williamson model of elastic contact between fractal surfaces. J. Mech. Phys. Solid. 54 (12), 2569–2591. https://doi.org/10.1016/j.jmps.2006.05.006.

Dickens, G.R., Wallace, P.J., Paull, C.K., et al., 2000. Detection of Methane Gas Hydrate in the Pressure Core Sampler (PCS): Volume-Pressure-Time Relations during Controlled Degassing Experiments, vol. 164. Texas A & M University College Station Tx, pp. 113–126. https://doi.org/10.2973/odp.proc.sr.164.210.2000.

Fulthorpe, C.S., Miller, K.G., Droxler, A.W., et al., 2008. Drilling to decipher long-term sea-level changes and effects—a joint consortium for ocean leadership, ICDP, IODP, DOSECC, and chevron workshop. Sci. Drill. 6 (6), 19–28. https://doi.org/10.2204/iodp.sd.6.02.2008.

Gao, M.Z., Xie, J., Guo, J., et al., 2021a. Fractal evolution and connectivity characteristics of mining-induced crack networks in coal masses at different depths[J]. Geomech. Geophys. Geo-Energy Geo-Resour. 7 (1), 9. https://doi.org/10.1007/s40948-020-00207-4.

Gao, M.Z., Chen, L., Fan, D., et al., 2021. Principle and technology of coring with in-situ pressure and gas maintaining in deep coal mine. J. China Coal Soc. 46 (03), 885–897 (in Chinese). https://doi.org/10.13225/j.cnki.jccs.YT21.0297.

Gao, M.Z., Liu, J.J., Lin, W.M., et al., 2020a. Study on in-situ stress evolution law of ultra-thick coal seam in advance mining. Coal Sci. Technol. 48 (2), 28–35(in Chinese).

Gao, M.Z., Xie, J., Gao, Y.N., et al., 2021b. Mechanical behavior of coal under different mining rates: a case study from laboratory experiments to field testing. Int. J. Mining Sci. Technol. 31 (5), 825–841. https://doi.org/10.1016/j.ijmst.2021.06.007.

Gao, M.Z., Zhang, J.G., Li, S.W., et al., 2020b. Calculating changes in the fractal dimension of surface cracks to quantify how the dynamic loading rate affects rock failure in deep mining. J. Cent. S. Univ. 27 (10), 3013–3024. https://doi.org/10.1007/s11771-020-4525-5.

Gao, M.Z., Zhang, Z.L., Yin, X.G, et al., 2018. The location optimum and permeability-enhancing effect of a low-level shield rock roadway. Rock Mech. Rock Eng. 51 (9), 2935–2948. https://doi.org/10.1007/s00603-018-1461-x.

He, Z.Q., Chen, L., Lu, T., et al., 2019. The optimization of pressure controller for deep earth drilling. Therm. Sci. 23. https://doi.org/10.2298/TSCI180612123H, 123-123.

He, Z.Q., Xie, H.P., Gao, M.Z., et al., 2020. Design and verification of a deep rock corer with retaining the in situ temperature. Adv. Civ. Eng. 2020 (11), 1–13. https://doi.org/10.1155/2020/8894286.

Hu, Y.Z., Tonder, K., 1992. Simulation of 3-D random rough surface by 2-D digital filter and fourier analysis. Int. J. Mach. Tool Manufact. 32 (1), 83–90. https://doi.org/10.1016/0890-6955(92)90064-N.

Ingrid, T., Martin, S., 2018. A review on challenges in the assessment of geo-mechanical rock performance for deep geothermal reservoir development. Renew. Sustain. Energy Rev. 82 (3), 3972–3980. https://doi.org/10.1016/j.rser.2017.10.076.

Lan, W.J., Wang, H.X., Zhang, X., et al., 2019. Sealing properties and structure optimization of packer rubber under high pressure and high temperature. Petrol. Sci. 16 (3), 632–644. https://doi.org/10.1007/s12182-018-0296-0.

Li, C., Xie, H.P., Gao, M.Z., et al., 2021. Novel designs of pressure controllers to enhance the upper pressure limit for gas-hydrate-bearing sediment sampling. Energy (5), 120405. https://doi.org/10.1016/j.energy.2021.120405.

Lyu, X.K., Yang, W.J., Xu, J.L., et al., 2015. The influence of characteristic of rough surface on gas sealing performance in seal structure. J. Mech. Eng. 51 (23), 110–115. https://doi.org/10.3901/JME.2015.23.110 (in Chinese).

Masjedi, M., Khonsari, M.M., 2015. On the effect of surface roughness in point-contact EHL: formulas for film thickness and asperity load. Tribol. Int. 82, 228–244. https://doi.org/10.1016/j.triboint.2014.09.010.

Milkov, A.V., Dickens, G.R., Claypool, G.E., et al., 2004. Co-existence of gas hydrate, free gas, and brine within the regional gas hydrate stability zone at Hydrate Ridge (Oregon margin): evidence from prolonged degassing of a pressurized core. Earth Planet Sci. Lett. 222 (3–4), 829–843. https://doi.org/10.1016/j.epsl.2004.03.028.

Mu, X., Sun, Q., Xu, J., et al., 2018. Feasibility analysis of the replacement of the actual machining surface by a 3D numerical simulation rough surface. Int. J. Mech. Sci. 150, 135–144. https://doi.org/10.1016/j.ijmecsci.2018.10.023.

Pang, X.Q., Jia, C.Z., Wang, W.Y., 2015. Petroleum geology features and research developments of hydrocarbon accumulation in deep petroliferous basins.

Petrol. Sci. 12 (1), 1–53. https://doi.org/10.1007/s12182-015-0014-0.
Ren, X., Wu, C.W., Zhou, P., 2010. Gas sealing performance study of rough surface. J. Mech. Eng. 46 (16), 176–181. https://doi.org/10.3901/JME.2010.16.176 (in Chinese).
Schultheiss, P., Holland, M., Humphrey, G., 2009. Wireline coring and analysis under pressure: recent use and future developments of the HYACINTH system. Sci. Drill. 7, 44–50. https://doi.org/10.2204/iodp.sd.7.07.2009.
Wan, H., Zhao, W., Hua, X., et al., 2019. Numerical study of influence of deep coring parameters on temperature of in-situ core. Therm. Sci. 23. https://doi.org/10.2298/TSCI180813209W, 209-209.
Wang, X.H., Li, X.Z., Cao, M.Y., et al., 2021. Study on surface effect of sheet metal with vibration excitation based on DEM. J. Plasticity Eng. 28 (2), 92–101. https://doi.org/10.3969/j.issn.1007-2012.2021.02.013 (in Chinese).
Whitehouse, D.J., Archard, J.F., 1971. The properties of random surfaces of significance in their contact. Proc. Royal Soc. A 316 (1524), 97–121. https://doi.org/10.1098/rspa.1970.0068.
Wu, N.H., Xie, H.P., Chen, L., et al., 2020. Sealing form and failure mechanism of deep in situ rock core pressure-maintaining controller. Geofluids 2020 (11), 1–15. https://doi.org/10.1155/2020/8892720.
Xie, H.P., Gao, M.Z., Zhang, R., et al., 2019. Study on the mechanical properties and mechanical response of coal mining at 1000m or deeper. Rock Mech. Rock Eng. 52, 1475–1490. https://doi.org/10.1007/s00603-018-1509-y.
Xie, H.P., Gao, M.Z., Zhang, R., et al., 2020. Study on concept and progress of in situ fidelity coring of deep rocks. Chin. J. Rock Mech. Eng. 39 (5), 865–876. https://doi.org/10.13722/j.cnki.jrme.2020.0138 (in Chinese).
Yang, L.W., Su, Y., Luo, J., et al., 2020a. Development and application of GW-CP194-80A pressure-maintaining coring tool. Nat. Gas. Ind. 40 (4), 91–96. https://doi.org/10.3787/j.issn.1000-0976.2020.04.011 (in Chinese).
Yang, M.Q., Xie, H.P., Gao, M.Z., et al., 2020b. On distribution characteristics of the temperature field and gas seepage law of coal in deep mining. Therm. Sci. 24 (6 Part B), 3923–3931. https://doi.org/10.2298/TSCI2006923Y.
Xie, H.P., Liu, T., Gao, M.Z., 2021. Research on in-situ condition preserved coring and testing systems. Petrol. Sci. https://doi.org/10.1016/j.petsci.2021.11.003.
Yang, X., Jackson, R.L., 2017. Statistical models of nearly complete elastic rough surface contact -comparison with numerical solutions. Tribol. Int. 105, 274–291. https://doi.org/10.1016/j.triboint.2016.10.003.
Yu, B., Xie, H., Chen, L., et al., 2020. Exploration of digital twin design mechanism of the deep in situ rock insulation coring device. Geofluids 2020 (1), 1–12. https://doi.org/10.1155/2020/8835085.
Zhao, F.L., Ai, C.Z., Yang, D.J., et al., 2006. Study on the evaluation method and evaluation parameters of cutting surface roughness of carbon/carbon composite. Acta Metrol. Sin. (3), 206–211. https://doi.org/10.3321/j.issn:1000-1158.2006.03.002 (in Chinese).